Cell Reports
Physical Science

CellPress
OPEN ACCESS

Article

Gold-templated covalent targeting of the CysSec-dyad of thioredoxin reductase 1 in cancer cells

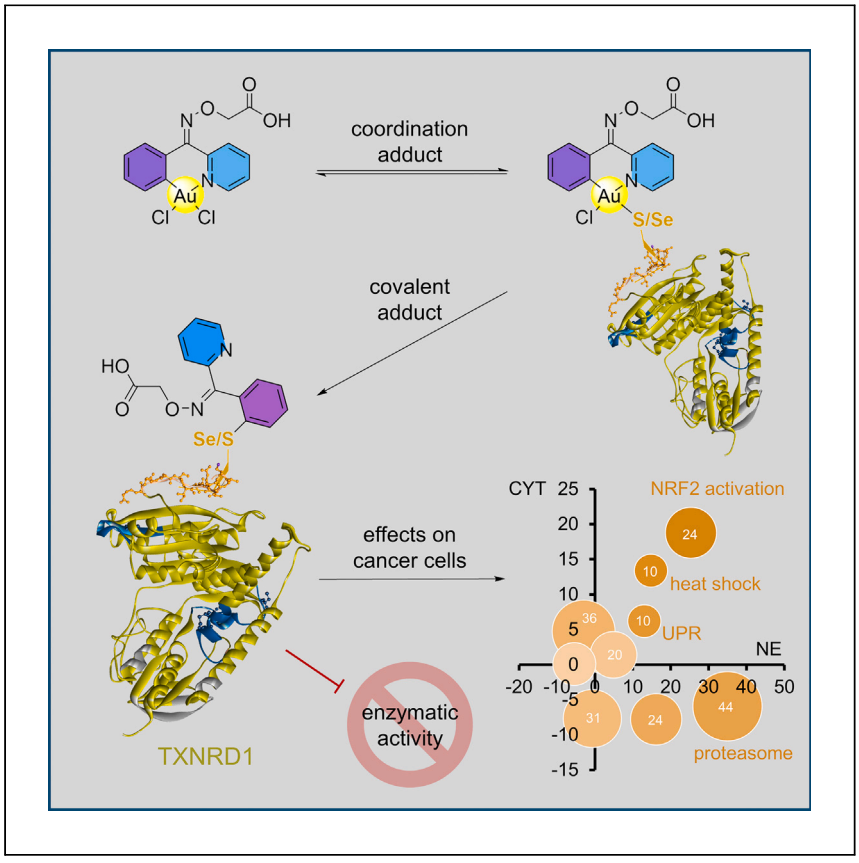

Skos et al. report a gold-templated, two-step covalent targeting mechanism that shows potential as an anticancer strategy. A C^N-cyclometalated gold(III) compound irreversibly targets TXNRD1 and inhibits its enzymatic activity in cell extracts by selective arylation, with dose-dependent, selective targeting of TXNRD1 demonstrated in cell lysates.

Lukas Skos, Claudia Schmidt, Sophie R. Thomas, ..., Christopher Gerner, Angela Casini, Samuel M. Meier-Menches

angela.casini@tum.de (A.C.)
samuel.meier-menches@univie.ac.at (S.M.M.-M.)

Highlights

A two-step, gold-templated covalent targeting mechanism is presented

A C^N-cyclometalated gold(III) compound irreversibly targets and inhibits TXNRD1

The CysSec-dyad of TXNRD1 is selectively targeted in a reducing environment

Skos et al., Cell Reports Physical Science 5, 102072
July 17, 2024 © 2024 The Author(s). Published by Elsevier Inc.
https://doi.org/10.1016/j.xcrp.2024.102072

Cell Reports
Physical Science

CellPress
OPEN ACCESS

Article

Gold-templated covalent targeting of the CysSec-dyad of thioredoxin reductase 1 in cancer cells

Lukas Skos,[1,2,9] Claudia Schmidt,[3,9] Sophie R. Thomas,[3] Mihyun Park,[3] Verena Geiger,[3] Dominik Wenisch,[4] Riccardo Bonsignore,[5] Giorgia Del Favero,[6,7] Thomas Mohr,[1] Andrea Bileck,[1,8] Christopher Gerner,[1,7,8] Angela Casini,[3,*] and Samuel M. Meier-Menches[1,4,8,10,*]

SUMMARY

Covalent drugs emerged as a promising addition to the arsenal of medicinal chemistry tools. Here, a gold-templated mechanism is exploited to enable the selective covalent targeting of the CysSec-dyad of thioredoxin reductase 1 (TXNRD1) in cancer cells. This two-step mechanism involves reversible coordination of a cyclometalated gold(III) compound, featuring a bidentate C^N ligand, to thiolates/selenolates, followed by reductive elimination and irreversible covalent cross-coupling reaction of the ligand to these nucleophiles. Following this reactivity, potent inhibition of TXNRD1 activity was shown *in vitro*, including cancer cell extracts. Selective arylation of the CysSec-dyad in the presence of reducing equivalents was seen in cell-free studies. Chemoproteomic studies showed that the proposed mechanism is selective toward specific protein targets, including TXNRD1. Proteome profiling revealed down-regulation of the detected selenoproteins, except TXNRD1, and induction of the NRF2-KEAP1 pathway. Metal-templated covalent targeting may prove useful to rationally expand the ligandable space of covalent drug discovery.

INTRODUCTION

Covalent drug discovery has made significant progress during the last decade.[1] Covalent inhibitors feature mildly reactive, electrophilic groups, including, among others, acrylamides, activated nitriles, or cyanamides.[2] Careful control of the reactivity of covalent warheads can achieve selectivity and prolong target engagement, thereby favorably altering pharmacodynamic profiles[3] of drug candidates to outperform classical non-covalent targeting strategies. The rational development of reactive covalent inhibitors had long been avoided in medicinal chemistry due to the perceived risks of off-target reactivity and their interference in biological assays.[1] Initial covalent drug discovery efforts were driven by incorporating reactive functional groups into known reversible inhibitors. For example, to overcome the T790M gatekeeper mutation in the EGF receptor of non-small cell lung cancer, afatinib was designed with an acrylamide moiety that reacts with Cys797 in the receptor and was approved in 2013.[4] More recent covalent drugs were discovered by electrophile-first approaches, such as sotorasib, a covalent inhibitor for KRAS(G12C) mutants.[5] Therefore, covalent target engagement is a promising strategy for hard-to-drug targets with shallow or cryptic binding pockets. Electrophile-first approaches are largely facilitated by chemoproteomic techniques.[6,7]

[1]Department of Analytical Chemistry, University of Vienna, Waehringer Str. 38, 1090 Vienna, Austria

[2]Doctoral School of Chemistry, University of Vienna, Waehringer Str. 38, 1090 Vienna, Austria

[3]Medicinal and Bioinorganic Chemistry, Department of Chemistry, School of Natural Sciences, Technical University of Munich, Lichtenbergstr. 4, 85748 Garching, Germany

[4]Institute of Inorganic Chemistry, University of Vienna, Waehringer Str. 42, 1090 Vienna, Austria

[5]Dipartimento di Scienze e Tecnologie, Biologiche, Chimiche, e Farmaceutiche, Università degli Studi di Palermo, 90128 Palermo, Italy

[6]Department of Food Chemistry and Toxicology, University of Vienna, Waehringer Str. 38, 1090 Vienna, Austria

[7]Core Facility Multimodal Imaging, University of Vienna, Waehringer Str. 38, 1090 Vienna, Austria

[8]Joint Metabolome Facility, University of Vienna and Medical University of Vienna, Waehringer Str. 38, 1090 Vienna, Austria

[9]These authors contributed equally

[10]Lead contact

*Correspondence: angela.casini@tum.de (A.C.), samuel.meier-menches@univie.ac.at (S.M.M.-M.)

https://doi.org/10.1016/j.xcrp.2024.102072

This is an open access article under the CC BY license (http://creativecommons.org/licenses/by/4.0/).

In this context, we decided to explore a medicinal inorganic chemistry approach, based on organogold compounds,[8] to develop anticancer metallodrugs acting via covalent bond formation reactions with pharmacological targets. Gold-based drugs are a class of metal-based anticancer agents[9] endowed with distinct modes of action (MoA) with respect to platinum-based anticancer agents,[10–14] and which can be categorized into gold(I) and gold(III) compound families that generally follow protein-targeting pathways, with a few remarkable exceptions.[15–17] Auranofin represents the benchmark gold(I) drug that was initially approved to treat rheumatoid arthritis and is currently being repurposed as an anticancer agent.[18] Among its validated modes of action, the inhibition of the selenoenzyme thioredoxin reductase 1 (TXNRD1) is particularly relevant,[19,20] since its selective inhibition can induce pro-apoptotic signals.[18,21] The metallodrug binding mode involves the formation of a reversible coordination bond to the selenocysteine in the protein's catalytically active site, following ligand exchange reactions at the gold(I) center.[19,22] Recently, it has been shown that gold(III) complexes may exert their anticancer activity by covalent targeting of proteins beyond the pure coordinative binding mode, and as such, emerge as new chemical tools for bioorthogonal transformations *in vitro* and *in vivo*, as well as novel drug leads.[23] For example, the anticancer gold(III) *meso*-porphyrin IX was shown to covalently modify protein cysteine thiols of TXN, peroxiredoxin (PRDX), and deubiquitinases.[24] In this example, the gold(III) center was crucial to activate the *meso*-carbons of the porphyrin ring toward nucleophilic substrates. In 2017, a study by Tanaka and co-workers reported on a cyclometalated gold(III) compound tethered to an *N*-glycoalbumin carrier, which by virtue of its Lewis acid character was capable of activating propargyl ester functions for binding to proteins by amide bond formation *in vivo*.[25] Some gold(III) organometallic compounds are also known to perform metal-templated covalent additions of ligands to biological nucleophiles, especially cysteine thiols.[26] In this context, we and others observed that cyclometalated gold(III) compounds featuring bidentate C^N ligands can template the formation of covalent aryl-peptide adducts via C–S cross-coupling at cysteine residues (Figure 1A).[21,27,28] According to density functional theory calculations combined with mass spectrometry (MS) studies, this involves a two-step reaction mechanism (Figure 1A).[29] First, the gold(III) coordinates to a thiolate/selenolate in *trans* position to the N-heterocycle of the C^N-cyclometalated ligand upon exchange with one of the ancillary ligands, forming a classical gold coordination bond. Second, a peptide bond nitrogen is required to exchange the N-heterocycle, which allows the C-S/Se cross-coupling reaction by reductive elimination. The reduced gold atom is released during this process. Interestingly, this gold-templated covalent reactivity was found to be selective toward thiols over other nucleophiles.[21] The mechanism combines the benefits of reversible coordination of gold(III) adducts for targeting thiol-based nucleophiles with the possibility of covalently modifying these sites. Such reactivity is unique to this family of organometallic gold(III) complexes and is not accessible by gold(I) compounds.[26,30,31]

Reactivity toward arylation can be tuned by structural changes of the chelating and ancillary ligands. [Au($C^{CO}N$)Cl_2] ($C^{CO}N$ = 2-benzoylpyridine; Figure 1B) was found to be more reactive than other C^N-cyclometalated derivatives.[29] Furthermore, cyclometalation is one of the main strategies to stabilize gold(III) centers, so that these compounds become sufficiently stable for potential medicinal applications or for functionalization for imaging and targeting purposes.[22,32]

Activity-based proteomic profiling of [Au($C^{CO}N$)Cl_2] in *Staphylococcus aureus* cell extracts showed that the compound can efficiently arylate cysteine thiol residues of >100 proteins, >50% of which were not engaged by the established

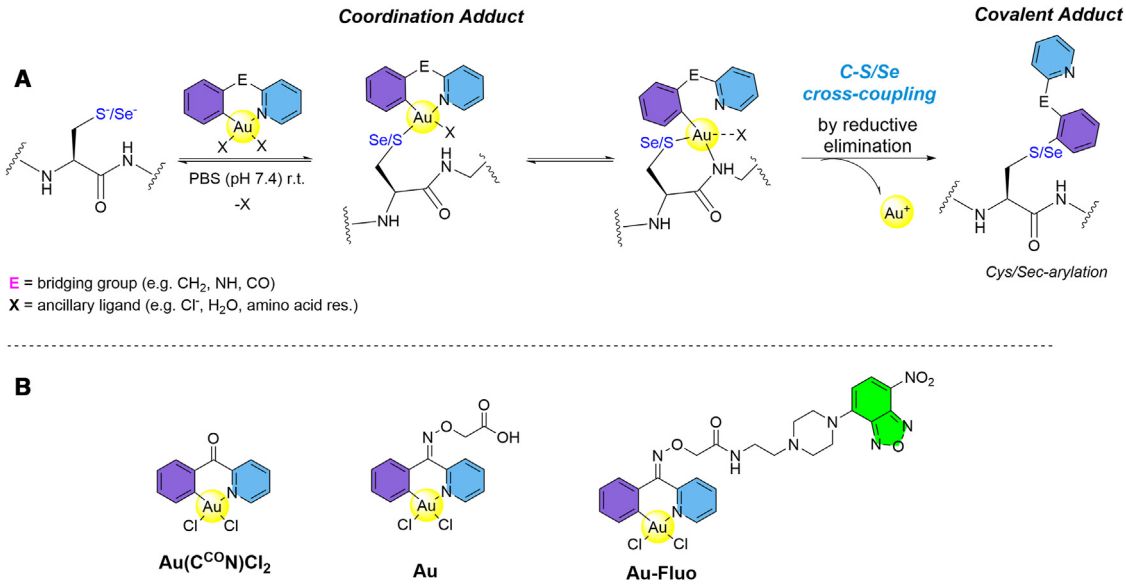

Figure 1. Mechanism of gold(III)-templated cross-coupling and chemical structures of the investigated compounds

(A) Proposed scheme of the reaction of C^N-cyclometalated gold(III) compounds with thiols and selenols of proteins. The binding proceeds via 2 steps: (1) the formation of a coordination adduct in which the gold(III) center binds directly to the S^-/Se^- nucleophiles and (2) C–S/Se cross-coupling reaction via reductive elimination and liberation of gold(0/I).

(B) Chemical structures of the parent compound [Au($C^{CO}N$)Cl_2] ($C^{CO}N$ = 2-benzoylpyridine) and of the investigated C^N-cyclometalated gold(III) analogs **Au** (with a functional carboxylic acid via an oxime) and **Au-Fluo**.

α-chloroacetamide.[33] Out of the ligandable sites, 10 potential arylation sites were assigned to be close to the respective functional protein sites; some of the identified proteins were already known targets for metal compounds with antibacterial effects.[33]

These initial results showed promise for gold(III)-templated covalent targeting as an anticancer strategy. Here, a cyclometalated gold(III) C^N complex featuring a carboxylic acid group on the ligand scaffold for further functionalization (**Au**, Figure 1B) was used to investigate metal-templated covalent targeting as an anticancer strategy in human SW480 colon cancer cells. In detail, we applied MS-based and complementary methods to validate the proposed reactivity. In general, besides other analytical techniques,[34–36] MS contributed toward elucidating the reactivity of metal-based candidates.[37–40] In the frame of increasingly mechanism-driven research,[41–43] metalloproteomic techniques were successfully established to characterize target landscapes,[41,44–51] metal interactomes,[52–54] or redox proteomes.[55] In this context, using chemoproteomic techniques, we saw target selectivity for TXNRD1 and found potent inhibition of TXNRD1 activity against the isolated enzyme and in cell extracts. In the presence of reducing equivalents, the CysSec-dyad of TXNRD1 was selectively arylated by **Au**, highlighting that selenocysteine may contribute to the coordinative targeting mechanism. Metal-templated covalent strategies may represent a promising strategy to expand the ligandable space in covalent drug discovery.

RESULTS AND DISCUSSION

The investigated C^N-cyclometalated gold(III) compounds template cross-coupling reactions to thiols

The parent substance [Au($C^{CO}N$)Cl_2] was modified to two oxime-containing C^N-cyclometalated compounds featuring either a functional carboxylic acid group (**Au**) or

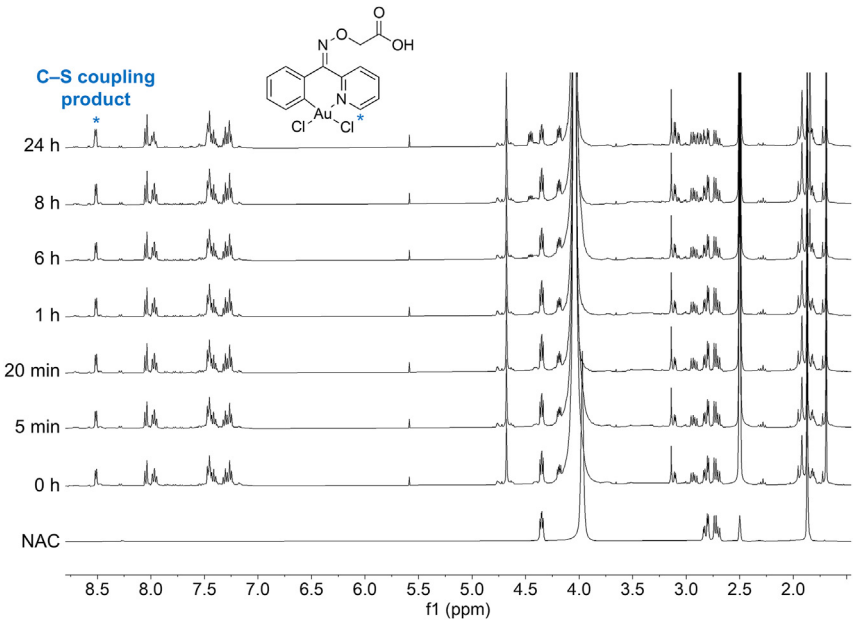

Figure 2. Reactivity of Au toward NAC

H-NMR spectra of **Au** reacting with 3 equiv of NAC in DMSO-d_6:D_2O (9:1). The spectrum of NAC alone is included as a reference. The characteristic shift of the α-H was observed (Δ = 0.78 ppm), indicating a rapid C–S coupling of **Au** with NAC.

a fluorescent tag (**Au-Fluo**). **Au** was synthesized according to a previously reported procedure.[52] The fluorescent derivative **Au-Fluo** was synthesized by amidation of **Au** with the 2-(-4-(7-nitrobenzo[*c*][1,2,5]oxadiazol-4-yl)piperazon-1-yl)ethane-1-amine fluorophore, and both compounds were characterized by standard analytical methods (Figures S1 and S2).

Since metal-based compounds are typically reactive molecules that can undergo ligand exchange reactions, the stability of the complexes **Au** and **Au-Fluo** was tested in DMSO-d_6:D_2O (9:1) by ^{1}H-NMR spectroscopy (Figures S3 and S4). The compounds were stable over 24 h under these conditions, as suggested by the observation of the characteristic doublet at 9.31 ppm for **Au** and **Au-Fluo**, corresponding to the proton adjacent to the Au-N bond in the pyridinyl ring (α-H).

Additionally, both compounds were investigated with respect to their ability to arylate thiols. The compounds were incubated under the same conditions in the presence of 3 equiv of *N*-acetylcysteine (NAC; Figures 2 and S5). The characteristic shift of the ^{1}H-NMR signal from 9.3 to 8.5 ppm of the α-H corresponding to thiol arylation[27] was observed for both **Au** and **Au-Fluo**. The kinetics of C–S bond formation varied only slightly, with **Au** inducing complete arylation within the timescale of the first measurement (time = 0 h), as also seen for [Au($C^{CO}N$)Cl_2] (Figure S6), whereas **Au-Fluo** required a few extra minutes.

Then, the interaction of **Au-Fluo** with BSA was studied using fluorescence spectroscopy. BSA represents a competitive binding model for **Au-Fluo** because it contains one free cysteine, several disulfide bridges, and several surface-exposed nucleophiles (e.g., imines) that can coordinate to the gold(III) center by ligand exchange. The luminescence properties of **Au-Fluo** were determined first (Figure 3A). The emission spectrum of **Au-Fluo** featured an excitation maximum at 493 nm and an

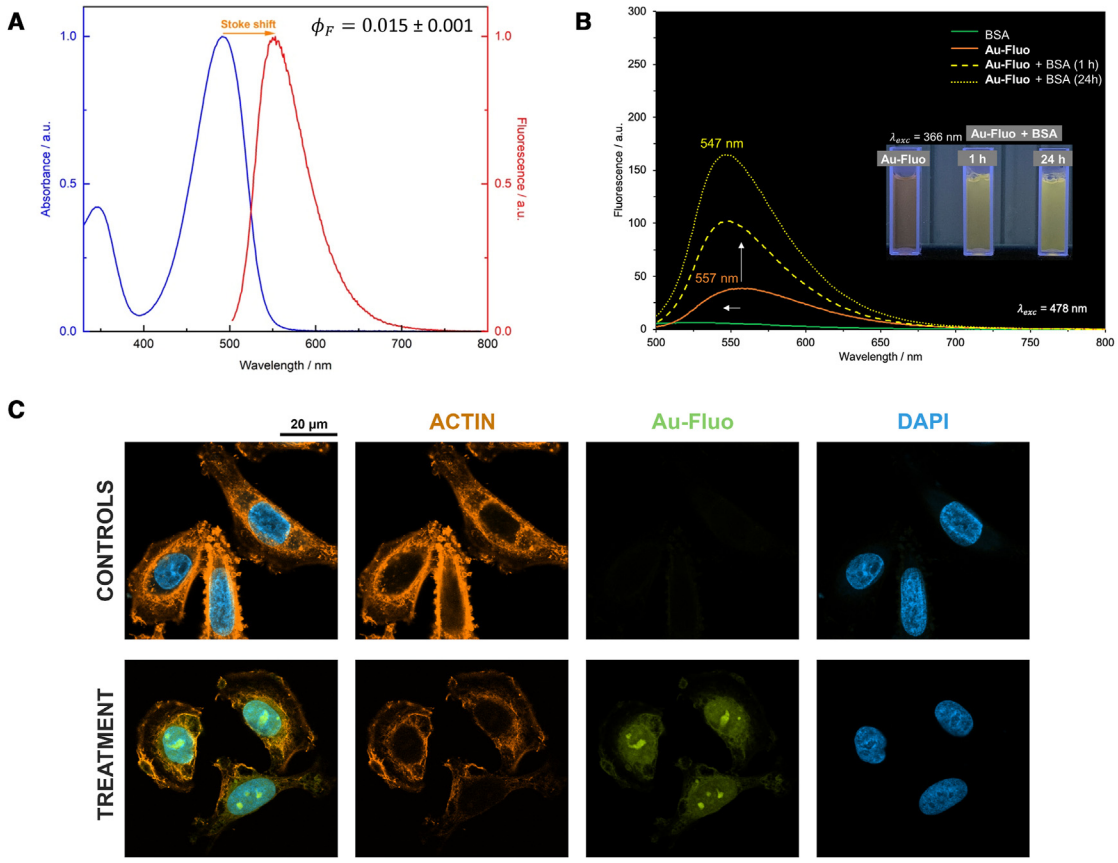

Figure 3. Fluorescence spectroscopy and microscopy studies of Au-Fluo

(A) Absorbance (blue, $\lambda_{abs,max}$ = 493 nm) and emission (red, $\lambda_{em,max}$ = 553 nm) spectrum of **Au-Fluo** in DMSO with the related Stokes shift (orange) of $\Delta\lambda$ = 62 nm, and the absolute fluorescence quantum yield (φ_F). For the emission spectrum, **Au-Fluo** was excited at the absorbance maximum of 493 nm.

(B) Fluorescence emission spectra recorded over time of the interaction between **Au-Fluo** (1 equiv) and BSA (10 equiv) at an excitation wavelength of 478 nm. Spectra were recorded in PBS (pH 7.4):DMSO (9:1), and samples were incubated at 37°C for 1 and 24 h. The spectra of BSA (green) and free **Au-Fuo** (orange) incubated for 24 h are also reported for comparison.

(C) Cellular distribution of **Au-Fluo** in SW480 cancer cells after a 4-h incubation studied by confocal fluorescence microscopy. DAPI (blue) indicates nuclei and phalloidin (red) indicates actin cytoskeleton. Green fluorescence of **Au-Fluo** was monitored after excitation at 469 nm and emission at 525 nm (GFP channel). Scale bar, 20 µm.

emission maximum at 553 nm in PBS:DMSO (9:1). For the study with BSA, 1 equiv of **Au-Fluo** and 10 equiv of BSA were dissolved in PBS (pH 7.4):DMSO (9:1) and incubated at 37°C for 1 and 24 h. Solutions of **Au-Fluo** and BSA at the same concentrations were analyzed as controls under the same conditions. Upon incubation for 1 h with BSA, the emission maximum underwent a blueshift toward 547 nm, indicating an arylation reaction potentially at the cysteine (Figure 3B). Most notably, the fluorescence intensity further increased by approximately 60% over 24 h.

The C^N-cyclometalated gold(III) compounds are moderately cytotoxic, and Au-Fluo distributes to the perinuclear and nuclear regions

The antiproliferative activity of the two compounds **Au** and **Au-Fluo** was determined in human SW480 colon cancer cells using the colorimetric MTT assay. Cells were incubated for 24 and 72 h. The compounds showed moderate cytotoxicity. The half-maximal effective concentration (EC_{50}) for growth inhibition was determined to be 62 ± 1 and 32 ± 6 µM for **Au** and **Au-Fluo**, respectively, after 24 h (Figure S7). After 72 h, the potency increased slightly to EC_{50} values of 31 ± 9 µM for **Au** and 20 ± 2 µM for **Au-Fluo**.

The fluorescence of **Au-Fluo** was further used to track its cellular distribution in SW480 cancer cells. Its excitation and emission spectra enabled excitation at 469 nm and data acquisition by green fluorescence in the microscope. For these studies, SW480 cells were treated with **Au-Fluo** at half-EC_{50} (16 μM) and EC_{50} (32 μM) concentrations for up to 24 h. The cellular distribution of **Au-Fluo** in SW480 cells was assessed by live-cell fluorescence microscopy (Figure S8). The medium had to be exchanged before analysis to reduce the background fluorescence. **Au-Fluo** was found to distribute into SW480 cancer cells, with a slight preference for the nuclear compartment after 4 h, and the distribution remained similar over 24 h. This experiment was repeated using confocal fluorescence microscopy benefiting from an increased resolution. After fixing and permeabilization, the cells were co-stained with phalloidin (red) as a marker for the actin cytoskeleton and with DAPI (blue) as a marker for the nucleus (Figure 3C). **Au-Fluo** was confirmed to distribute to the perinuclear region and into the nuclear compartment.

TXNRD1 is identified as a potential target of Au in SW480 cancer cell extracts

The gold-templated covalent targeting of **Au** was then investigated in the proteome of SW480 cancer cells using a chemoproteomics approach.[41,45] Coupling conditions of the carboxylate-containing **Au** to the amine-based Sepharose resin were optimized. The amidation reaction turned out to proceed selectively in an aqueous solution in the presence of 1.5 equiv of 1-ethyl-3-(3-dimethylaminopropyl) carbodiimide at pH 4 when using **Au** and 1 equiv of serotonin as a model amine. Amidation required at least 18 h to proceed, which led to the hydrolysis of one chlorido ligand at the gold(III) center and formation of a gold(III)-hydroxido complex, as detected by ion trap MS at *m/z* 661.11 (m_{theor} = 661.09) with a characteristic single chloride isotope pattern (Figure S9). These coupling conditions were employed for immobilizing **Au** on amine-containing Sepharose resins, but using a 3-fold excess of **Au** with respect to the available amines to increase the coupling efficiency. Since the buffer of the chemoproteomic experiment contained DTT as a reducing agent, the reactivity of **Au** toward DTT (1:2 equiv) was also investigated over the course of 70 min directly after mixing (Figure S10). In line with expectations, **Au** coordinated rapidly to DTT, but the cross-coupling reaction between the ligand and DTT progressed steadily over the entire incubation period. This indicated that DTT blocks immobilized **Au** only to a minor degree during the 2-h incubation of the chemoproteomic experiment since the coordination bond enables successive ligand exchanges until a final nucleophile traps the gold(III) complex.

The chemoproteomic experiment was performed using a differential approach (Figure 4A). The immobilized **Au** on Sepharose resin was exposed to a native protein whole-cell lysate of SW480 cancer cells for 2 h. During this time, the immobilized **Au** coordinates to nucleophiles under competitive conditions until a final nucleophilic moiety traps the complex and leads to an irreversible covalent bond. This approach is prone to non-selective binding of proteins to the resin due to hydrophobic interactions. To account for the latter, a separate competitive pull-down experiment was performed, where the native whole-cell lysate was pre-incubated for 2 h with free **Au** (12 μM) and then incubated for another 2 h with the **Au**-anchored resin. Pre-incubation with free **Au** leads to the irreversible arylation of potential interactors, which cannot be captured by the immobilized **Au** any longer, so that only non-selective interactors are detectable. Differences between the normal and the competitive pull-down reveals selective binding partners. Since we expected only covalently bound proteins to be attached to the resin after chemoselective arylation, we performed the proteolytic digestion directly on the beads, subsequent to harsh washing steps. After nano liquid chromatography-tandem MS (nLC-MS/MS)-based

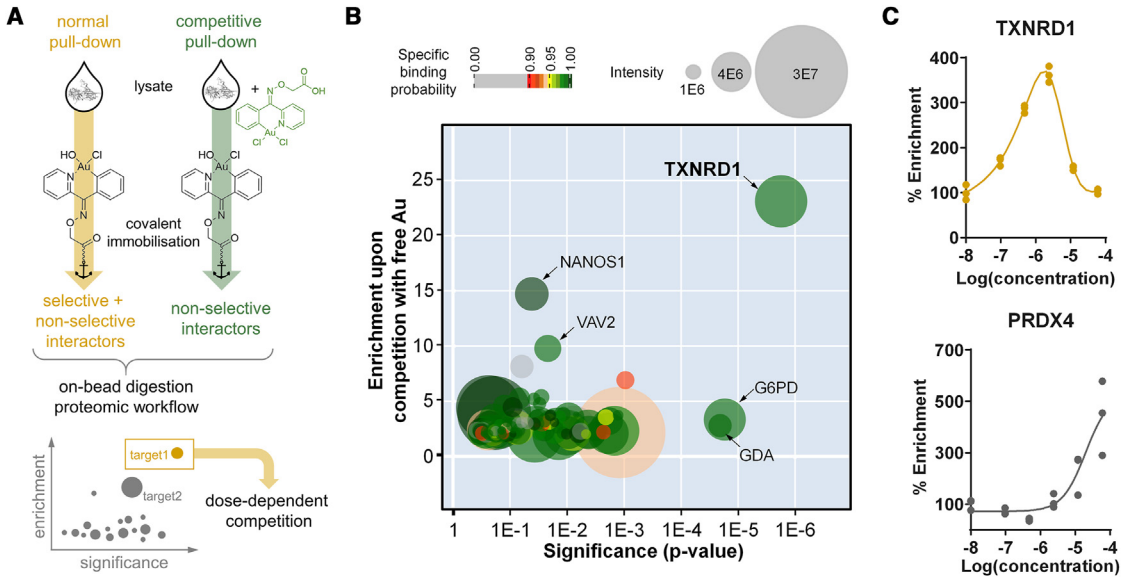

Figure 4. Target identification of immobilized Au using chemoproteomics

(A) **Au** was immobilized on amine Sepharose beads. Native protein cell lysates of SW480 cancer cells were prepared and either directly incubated with the immobilized probe (normal pull-down) or pre-treated with free **Au** (12 μM, competitive pull-down).

(B) Differential analysis of the normal and competitive pull-down experiments revealed selective binding to TXNRD1 from the native protein whole-cell lysate of SW480 cancer cells.

(C) Dose-dependent titration with free **Au** at 0 nM, 96 nM, 480 nM, 2.4 μM, 12 μM, and 60 μM revealed dose-dependent binding affinity for only TXNRD1 and PRDX4. The unusual titration curve indicates bis-arylation of TXNRD1 by **Au** possibly involving the CysSec-dyad. Each concentration was performed in 3 replicates.

proteomic analysis and evaluation, the potentially selective interactors were ranked by means of their enrichment efficiency and significance of interaction as calculated from the respective intensities in the normal and competitive pull-down (Figure 4B). A total of 2,833 proteins were identified in the pull-down from the whole-cell lysate of SW480 cancer cells. Strikingly, we identified the selenoprotein TXNRD1 as the most prominent selective interactor based on enrichment and significance (Figure 4B). TXNRD1 is a key player in the maintenance of the intracellular redox homeostasis within the TXN system, often overexpressed in cancers due to a constitutive activation of the transcription factor and stress sensor NRF2.[56] It is involved in apoptosis induction and has emerged as one of the main targets of cytotoxic gold complexes, including the clinically evaluated auranofin.[19,30,57] Human TXNRDs are homodimers coupled head to tail, each one containing a redox-active CysSec-dyad with sequential cysteine and selenocysteine residues at the C terminus responsible for the interaction of the enzyme with various substrates as well as TXN itself.[58]

The chemoproteomic approach was expanded to a dose-dependent competition experiment to verify the interaction with TXNRD1 and assess the potency of interaction.[47] This was achieved by titrating **Au** at increasing concentrations (0.096–60 μM) in the competitive pull-down. Once more, TXNRD1 was verified as an interactor of **Au** and showed a clear dose-dependent profile. However, in contrast to earlier observations,[47] we noted an unusual interaction profile suggesting that arylation of TXNRD1 by **Au** involves a second binding site. A 2:1 binding stoichiometry between **Au** and TXNRD1 was indicated by the apparent enrichment of TXNRD1 after the first arylation step, with a maximum at 2.4 μM and a nearly complete competition at 12 μM (Figure 4C). The catalytic CysSec-dyad of TXNRD1 potentially allows for two arylation events to occur. A further dose-dependent interaction was observed

with PRDX4, but only at the highest tested concentrations. PRDX4 is thus an unlikely target at pharmacologically relevant concentrations. It is worth noting that we did not observe other proteins with clear-cut dose-dependent profiles in the tested concentration range.

Au selectively arylates the catalytic CysSec-dyad on TXNRD1 in the presence of reducing equivalents

The selectivity of **Au** toward TXNRD1 in the chemoproteomic approach suggested the catalytic CysSec-dyad as a likely site of interaction and potentially enabling bis-adduct formation to occur. To characterize the terminal arylation sites, TXNRD1 was reacted with **Au** in a cell-free experiment using 0, 1, and 5 equiv of **Au**. Additionally, TXNRD1 was reacted with 1 equiv **Au** in the presence of 0, 1, and 5 equiv of NADPH as a reducing agent. Each sample was directly proteolytically digested and analyzed by nLC-MS/MS. To automatically detect modified peptides of TXNRD1 using MaxQuant (version 1.6.17.0), arylation and carbamidomethylation were customized as variable modifications on cysteine and selenocysteine. These experiments revealed a 96% sequence coverage of TXNRD1, including the C-terminal peptide that contains the catalytic CysSec-dyad (Figures 5A and S11A). The latter contained the sequence RSGASILQAGCUG (*m/z* 692.7775 [z = 2], m_{theor} = 692.7810) that showed a retention time (RT) of 28.2 min in this experimental setup (Figure 5B). Interestingly, already at a 1:1 molar ratio between TXNRD1 and **Au** in the absence of NADPH, two chromatographic signals for the arylated peptide (*m/z* 791.3072 [z = 2], m_{theor} = 791.3058) were observed, with RTs of 39.9 and 40.3 min, respectively. This indicated the presence of two distinct arylation sites on this peptide. Additionally, a bis-arylation product was observed (*m/z* 593.5517 [z = 3], m_{theor} = 593.5551) at RT = 49.1 min, supporting the possibility of two different binding sites on this peptide. The isotopic patterns of the different mass signals clearly showed the presence of selenium, revealing excellent simulation matches and mass accuracies of <5 ppm (Figures 5C and S11B). The four detected mass signals corresponding to the unmodified CysSec-dyad peptide (RT = 28.2 min), the two mono-arylated peptides (RT = 39.9 and 40.3 min), and the bis-arylated peptide (RT = 49.1 min) were individually selected for MS/MS analysis at their respective RTs (Figure 5D). MS/MS analysis revealed detailed information about the peptide sequence and the location of the arylation sites. The unmodified peptide was identified with characteristic b- and y-fragments.[40,59] The b_{11}^+ fragment represents an unmodified cysteine, while y_3^+ represents the unmodified C-terminal CUG fragment of this peptide. Interestingly, the b-fragments remained similar for the mono-arylated product at 40.3 min, including the b_{11}^+ fragment. In contrast, the detected y-fragments indicated an arylation product, and the arylated y_2^+ fragment [$y_2(Ar)^+$] provided direct proof of selenocysteine arylation on TXNRD1. The second mono-arylation product eluting at RT = 39.3 min did not feature the unmodified b_{11}^+ ion. Indeed, the lack of the b_{11}^+ ion and the detection of an arylated b_{11}^+ ion ($b_{11}(Ar)^+$) highlights that this species corresponds to a cysteine arylation product. Finally, the MS/MS spectrum of the bis-arylation product eluting at 49.1 min revealed a different set of fragments that supported simultaneous cysteine and selenocysteine arylation. For example, the fragments $y_2(Ar)^+$ and $y_3(2Ar)^+$ clearly evidenced bis-arylation of the CysSec-dyad of TXNRD1. This terminal peptide was neither observed unmodified or arylated in the proteome profiling experiments of SW480 cancer cells treated with **Au**. In addition to their characteristic *m/z* ratios, RTs, and fragmentation spectra, these C-terminal peptides also featured distinct ion mobilities supporting the structural impact of the arylation on the peptide (Figure S11C).

The reaction between TXNRD1 and **Au** in the absence of NADPH also revealed three other arylated peptides, among which was an N-terminal peptide containing the

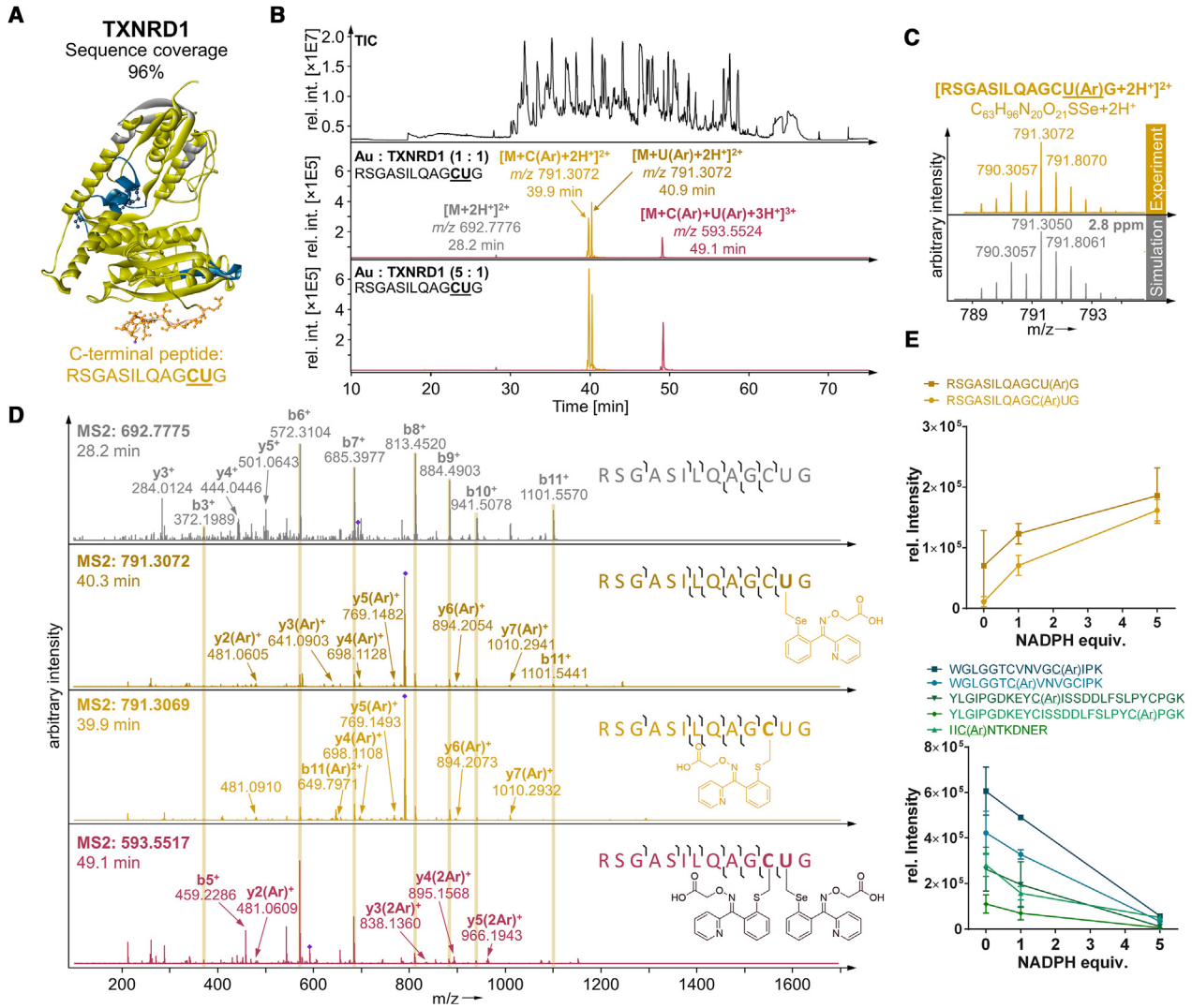

Figure 5. Identification of Au-templated arylation sites on TXNRD1

TXNRD1 (5 μg, 2.25 μM) was reacted with 0, 1, and 5 equiv of **Au** for 24 h. In a second setup, TXNRD1 was similarly reacted with 1 equiv of **Au** in the presence of 0, 1, and 5 equiv NADPH. Results are representative of 3 replicates. The protein was proteolytically digested and analyzed by nLC-MS/MS.

(A) A 96% sequence coverage of TXNRD1 was obtained.

(B) The chromatograms depict the total ion chromatogram, as well as the extracted ion chromatograms of the CU-containing C-terminal peptide. The reaction of TXNRD1 with **Au** in the absence of NADPH led to the arylation of the CysSec-dyad on TXNRD1. C- and U-arylations were observed at both molar ratios, as well as bis-arylations.

(C) The experimental mass signal and theoretical simulation of the isotope pattern of the mono-arylated C-terminal CU-containing peptide is shown.

(D) MS/MS experiments of the unmodified and covalently modified CysSec-dyad containing peptide unambiguously identified the location of the arylation sites on C and U.

(E) Increasing equivalents of NADPH (0, 1, 5 equiv) in the reaction between TXNRD1 and **Au** (1:1 equiv) led to an increase in the intensity of the arylation of the C-terminal CU-containing peptide, while all other arylated peptides considerably decreased in intensity. Data are shown as mean ± SD (n = 3).

CVNVGC motif that is known to coordinate gold (Figures 5E, S11D, and S11E).[60] These arylated species also increased in intensity with increasing **Au** equivalents. Interestingly, increasing equivalents of NADPH reduced the arylation efficiency on these sites, while at the same time the arylation of the C-terminal CysSec-containing peptide increased. This highlighted the selectivity of the gold-templated covalent targeting toward the C-terminal CysSec-dyad in the presence of reducing equivalents.

Au inhibits TXNRD1 activity

TXNRD1 activity was investigated to confirm the inhibitory effect of **Au** at the CysSec-dyad on enzymatic activity. **Au** was first tested against purified mammalian TXNRD1 and then against TXNRD1 in human A549 lung cancer cells. The cellular assays were performed in A549 cancer cells due to their abundant TXNRD1 expression, which is crucial for the sensitivity of the assay.[61] **Au** exhibits half-maximal inhibitory concentration (IC_{50}) values toward the isolated enzyme in the nanomolar range, corresponding to 0.069 $\pm$ 0.046 and 0.176 $\pm$ 0.045 μM at 15 and 75 min incubation time, respectively (Figure S12). **Au** is less potent than auranofin, showing an IC_{50} = 16 nM in the same experimental setup[62,63] but in line with previous studies on analogous cyclometalated gold(III) C^N complexes.[39,62] **Au** was then incubated with A549 cancer cells for 24 h, after which the cells were homogenized and the cell lysate extracted to determine the remaining TXNRD1 activity at different **Au** concentrations. **Au** inhibited the TXNRD1 activity *in cellulo* with an IC_{50} = 11.9 $\pm$ 3.8 μM. These results indicate that **Au** inhibits TXNRD1 activity in sufficiently low concentrations to account for its anticancer activities. Interestingly, the inhibitory concentration of **Au** *in cellulo* parallels the findings of the pull-down during dose-dependent competition (Figure 4C).

Overall, these data, together with the aforementioned chemoproteomic and MS studies, point toward the possible finding of **Au** as a metallodrug lead compound that exhibits an unprecedented mode of covalent TXNRD1 inhibition, compared to known covalent TXNRD1 inhibitors, including Ethaselen,[64] *TRi* compounds,[65] the half-mustard 2-chloroethyl ethyl sulfide,[66] cyclic selenylsulfides,[67] and other small molecules.[68,69]

Au treatment induces the NRF2-KEAP1 pathway, a key regulator of redox management capacity in cancer cells

The effects of sub-cytotoxic **Au** treatment (12 μM, 24 h) on SW480 cancer cells were evaluated by proteome profiling. The cytoplasmic (CYT) and nuclear (NE) protein fractions were separately processed and analyzed according to an established workflow using a data-dependent label-free quantification strategy.[70] A total of 4,347 protein groups were identified. As shown in Figure 6A, the correlation among biological replicates was typically around 0.85, as exemplified for two Au-treated NE fractions. This led to a clear separation of the proteome profiles of the different conditions, as revealed by principal-component analysis (Figure S13). Therein, the controls, **Au** treatments, and CYT and NE fractions were clearly separated, while the intra-condition replicates clustered together, indicating homogeneous treatment effects even in subcellular fractions. Of the total number of proteins, 117 and 465 protein groups were significantly regulated in the CYT and NE fractions, respectively (Figure S13B). Statistical significance was calculated using multiple testing-corrected *p* values based on 5% false discovery rate (FDR = 0.05 and S0 = 0.1). **Au** treatment induced heme oxygenase 1 (HMOX1), sulfiredoxin 1 (SRXN1), and heat shock 70-kDa protein 1A (HSPA1A) considerably in the CYT fraction. The induction of HSPA1A is also depicted in the profile plot highlighting the stability of the entire experiment (Figure 6B). Although **Au** targets TXNRD1, this protein was not found to be significantly regulated according to label-free quantification (LFQ) abundance (Figure 6B). The second putative binding partner PRXD4 was present in similar abundance and was also not significantly regulated (Figure 6C). Selenoprotein expression is known to depend on selenium availability.[71,72] **Au** treatment led to the significant down-regulation of the three detected selenoproteins glutathione peroxidase 1 (GPX1), GPX4, and the mitochondrial protein adenylyltransferase SelO (SELO), which may be explained by the reduction of the available intracellular selenium

CellPress
OPEN ACCESS

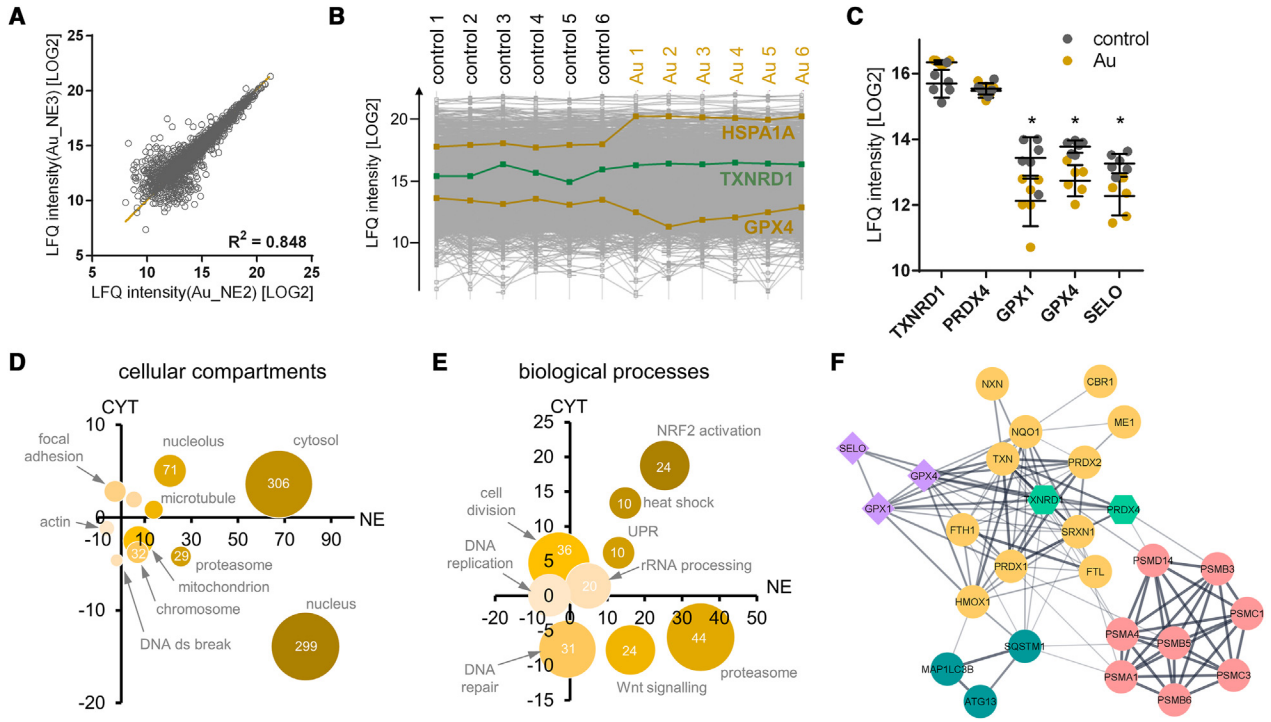

Figure 6. Effects of targeting TXNRD1 by Au in SW480 cancer cells

SW480 cancer cells were treated at sub-cytotoxic concentration of **Au** (12 μM, 24 h, $n = 6$). The protein content was fractionated into CYT and NE extracts and processed according to a data-dependent LC-MS/MS proteomics workflow.

(A) The scatterplot shows the distribution of the detected proteins according to the intensity of 2 representative biological replicates of nuclear extracts of **Au**-treated cells.

(B) The profile plot highlights the stability of protein abundance among biological replicates by visualizing the LFQ intensities of HSPA1A (significantly up-regulated), TXNRD1 (not regulated), and GPX4 (significantly down-regulated).

(C) While the selenoproteins GPX1, GPX4, and SELO are significantly down-regulated upon treatment, the potential targets TXNRD1 and PRDX4 are not. Significant protein regulations (*$p < 0.05$) were obtained after multiple testing correction using anFDR of 0.05 and S0 = 0.1. Data are represented as means and SDs ($n = 6$), including all individual data points.

(D) The significantly regulated proteins were grouped according to cellular compartment and visualized by plotting the summed $\log_2$(fold changes) according to CYT and NE. The size of the bubbles represents the number of regulated proteins in the group.

(E) The regulated proteins were also grouped according to biological processes and similarly visualized.

(F) The target-response network depicts the regulated proteins around the potential binding partners TXNRD1 and PRDX4, indicating effects on redox homeostasis (gold circles), protein degradation via the proteasome (rose circles), selenoproteins (purple diamonds), and autophagy (turquoise circles). Circle, up-regulated protein; diamond, down-regulated protein; hexagon, not regulated. Significantly regulated proteins were multiple testing corrected using a 5% FDR and S0 = 0.1.

pool after **Au** treatment. Selenium deficiency is known to lead to selenoprotein truncation, as a consequence of misinterpreting UGA as a normal stop codon instead of a codon for selenocysteine, and subsequent degradation by the proteasomal system.[73] It is probable that TXNRD1 remains unaffected because selenocysteine is located close to the C terminus.

The global effects of **Au** on the proteome of SW480 cancer cells were further illustrated by grouping the significantly regulated proteins according to Gene Ontology cellular compartments and biological processes, and plotting their summed fold changes according to CYT and NE fractions. We found cytosolic, nuclear, and nucleolar proteins to be the main disturbed cellular compartments (Figure 6D). Additionally, there seems to be a minor impact on mitochondria. The biological processes revealed the induction of NRF2 target genes as the strongest perturbation in both CYT and NE (Figures 6E; Table S1).[56,74] This is accompanied by the induction of HSPs and

an endoplasmic reticulum-based unfolded protein response, which is indicative of proteotoxic stress possibly due to non-specific gold-templated arylation reactions or the effects of the liberated gold(0/I) ions in these cells. Similarly to a previously reported gold(I) bis-N-heterocyclic carbene compound,[70] the proteasome was observed to be translocated into the nucleus. This may also be the consequence of proteotoxic stress. Indeed, we found the accumulation of green fluorescence from **Au-Fluo** in the nucleus by confocal microscopy (Figure 3C). These findings are supported by an analogous pathway representation with similar findings (Figure S13C).

The target-response network highlights the significantly regulated proteins in the neighborhood of the target protein TXNRD1 and PRDX4 (hexagons, Figure 6F). These proteins are located in the center of the network surrounded by a cluster of NRF2-induced redox proteins (yellow, e.g., HMOX1, SRXN1, TXN, PRDX1, and NADPH dehydrogenase [quinone] 1). The down-regulated selenoproteins GPX1, GPX4, and SELO (purple) are directly connected to these redox proteins and TXNRD1 as well. Autophagy-related proteins (turquoise, e.g., sequestosome 1 and autophagy-related protein 13) and proteasomal proteins (rose, e.g., proteasomal subunit alpha type-1 [PSMA1], PSMA4, and beta type-5), which digest irreversibly damaged proteins, were also found up-regulated. Therefore, **Au**-templated covalent targeting of TXNRD1 seems to impact proteins involved in maintaining the redox balance of SW480 cancer cells. As a consequence, cells try to cope with this challenge by inducing an NRF2 stress response and translocating the proteasome to the nuclear compartment. We further evaluated the induction of reactive oxygen species (ROS) in living SW480 cells by the **Au** treatment (2 h incubation). **Au** did not lead to ROS formation in this time interval in concentrations up to EC_{50} values (Figure S14).

To functionally evaluate the dependence of SW480 cancer cells on the induction of the NRF2 stress response upon treatment with **Au**, we tested for synergism[75] by co-treatment with the HMOX1 inhibitor OB-24.[76] HMOX1 was the most strongly up-regulated protein of the NRF2 target genes upon treatment with **Au** in both CYT and NE fractions (Figure S13C). HMOX1 protects cells from oxidative stress and has anti-apoptotic properties.[77] After determining the individual EC_{50} profiles of **Au** and OB-24 in SW480 cancer cells after 72 h of incubation, combination treatments were performed according to 0, EC_{10}, EC_{25}, EC_{50}, EC_{75}, and EC_{90} concentrations, for a total of 36 combinations. At EC_{75} concentrations of **Au**, a strong synergism (δ score >30) was observed with EC_{10} and EC_{25} concentrations of OB-24 (Figure S15). This verified the dependence of SW480 cancer cells on inducing the NRF2 stress response to cope with the TXNRD1-targeting ability of **Au**.

In summary, a cyclometalated gold(III) C^N complex is shown that covalently targets the CysSec-dyad of the selenoprotein TXNRD1 via a gold-templated reactivity. Using combined chemoproteomic and complementary methods, we have shown that this mechanism allows selective targeting of TXNRD1 in cancer cells by **Au**, leading to the potent inhibition of TXNRD1 activity. A fluorescent derivative of the title compound (**Au-Fluo**) enabled the investigation of the cellular distribution by fluorescence microscopy, showing that the compound can be efficiently taken up by cancer cells, and distributed to the perinuclear region and into the nuclear compartment. Although **Au** does not influence TXNRD1 abundance, significant proteome changes were found to be associated with maintaining the cellular redox balance. These changes were characterized by the down-regulation of the remaining selenoproteins and the induction of NRF2-derived redox proteins, but without accompanying ROS formation in SW480 cancer cells. Synergism studies revealed that the induction of

the NRF2 pathway is necessary for cancer cell survival upon treatment with **Au**. This metal-templated covalent targeting, fostering the formation of C–S/Se covalent bonds, can be used to design improved anticancer organogold candidates for covalent drug discovery. Furthermore, recent reports on the *in vitro*/*in vivo* anticancer effects of this family of cyclometalated gold(III) C^N complexes[78–82] could be revisited to consider this bioorthogonal reactivity as part of the compounds' MoA.

EXPERIMENTAL PROCEDURES

Resource availability

Lead contact

Further information and requests for resources should be directed to and will be fulfilled by the lead contact, Samuel M. Meier-Menches (samuel.meier-menches@univie.ac.at).

Materials availability

All materials generated in this study are available from the lead contact without restriction.

Data and code availability

The MS proteomics data have been deposited to the ProteomeXchange Consortium via the PRIDE partner repository with the dataset identifier PRIDE: PXD044971 (pull-down) and PRIDE: PXD044966 (profiling).

SUPPLEMENTAL INFORMATION

Supplemental information can be found online at https://doi.org/10.1016/j.xcrp.2024.102072.

ACKNOWLEDGMENTS

The authors are grateful to the Core Facility for Mass Spectrometry, the Core Facility Multimodal Imaging (Faculty of Chemistry, University of Vienna), and the Joint Metabolome Facility (University of Vienna and Medical University of Vienna), which are all members of the Vienna Life-Science Instruments. S.M.M.-M. acknowledges financial support from the Austrian Science Fund (P33238-N). S.R.T. acknowledges the TUM Global Postdoc Fellowship Scheme for funding. The authors thank Endre Kiss for helpful assistance during the confocal microscopy experiments.

AUTHOR CONTRIBUTIONS

Conceptualization, A.C. and S.M.M.-M. Methodology, L.S., C.S., C.G., A.C., and S.M.M.-M. Formal analysis, T.M., A.B., and C.G. Investigation, L.S., C.S., S.R.T., M.P., V.G., D.W., R.B., and G.D.F. Resources, G.D.F., C.G., A.C., and S.M.M.-M. Data curation, L.S., T.M., A.B., C.G., and S.M.M.-M. Writing – original draft, L.S., C.S., A.C., and S.M.M.-M. Writing – review and editing, all authors. Supervision, C.G., A.C., and S.M.M.-M.

DECLARATION OF INTERESTS

The authors declare no competing interests.

Received: October 18, 2023
Revised: May 3, 2024
Accepted: June 7, 2024
Published: June 28, 2024

REFERENCES

1. Boike, L., Henning, N.J., and Nomura, D.K. (2022). Advances in covalent drug discovery. Nat. Rev. Drug Discov. *21*, 881–898. https://doi.org/10.1038/s41573-022-00542-z.

2. Ertl, P., Altmann, E., and McKenna, J.M. (2020). The most common functional groups in bioactive molecules and how their popularity has evolved over time. J. Med. Chem. *63*, 8408–8418. https://doi.org/10.1021/acs.jmedchem.0c00754.

3. Lagoutte, R., Patouret, R., and Winssinger, N. (2017). Covalent inhibitors: An opportunity for rational target selectivity. Curr. Opin. Chem. Biol. *39*, 54–63. https://doi.org/10.1016/j.cbpa.2017.05.008.

4. Yu, H.A., and Pao, W. (2013). Targeted therapies: Afatinib-new therapy option for EGFR-mutant lung cancer. Nat. Rev. Clin. Oncol. *10*, 551–552. https://doi.org/10.1038/nrclinonc.2013.154.

5. Skoulidis, F., Li, B.T., Dy, G.K., Price, T.J., Falchook, G.S., Wolf, J., Italiano, A., Schuler, M., Borghaei, H., Barlesi, F., et al. (2021). Sotorasib for lung cancers with KRAS p.G12C mutation. N. Engl. J. Med. *384*, 2371–2381. https://doi.org/10.1056/NEJMoa2103695.

6. Mullard, A. (2023). Chemoproteomic trailblazer advances covalent candidate into the clinic, pushes allosteric agenda. Nat. Rev. Drug Discov. *22*, 689–690. https://doi.org/10.1038/d41573-023-00133-6.

7. Hacker, S.M., Backus, K.M., Lazear, M.R., Forli, S., Correia, B.E., and Cravatt, B.F. (2017). Global profiling of lysine reactivity and ligandability in the human proteome. Nat. Chem. *9*, 1181–1190. https://doi.org/10.1038/nchem.2826.

8. Casini, A., and Pöthig, A. (2024). Metals in cancer research: Beyond platinum metallodrugs. ACS Cent. Sci. *10*, 242–250. https://doi.org/10.1021/acscentsci.3c01340.

9. Boros, E., Dyson, P.J., and Gasser, G. (2020). Classification of metal-based drugs according to their mechanisms of action. Chem *6*, 41–60. https://doi.org/10.1016/j.chempr.2019.10.013.

10. Moreno-Alcántar, G., Picchetti, P., and Casini, A. (2023). Gold complexes in anticancer therapy: From new design principles to particle-based delivery systems. Angew. Chem. Int. Ed. *62*, e202218000. https://doi.org/10.1002/anie.202218000.

11. Mora, M., Gimeno, M.C., and Visbal, R. (2019). Recent advances in gold–NHC complexes with biological properties. Chem. Soc. Rev. *48*, 447–462. https://doi.org/10.1039/c8cs00570b.

12. Casini, A., Wai-Yin Sun, R., and Ott, I. (2018). Medicinal chemistry of gold anticancer metallodrugs. In Metallo-Drugs: Development and Action of Anticancer Agents, (De Gruyter), pp. 199–218. https://doi.org/10.1515/9783110470734-007.

13. Yue, S., Luo, M., Liu, H., and Wei, S. (2020). Recent advances of gold compounds in anticancer immunity. Front. Chem. *8*, 543. https://doi.org/10.3389/fchem.2020.00543.

14. Nardon, C., Boscutti, G., and Fregona, D. (2014). Beyond platinums: Gold complexes as anticancer agents. Anticancer Res. *34*, 487–492.

15. Schmidt, C., and Casini, A. (2022). Organometallic chemistry of gold-based drugs. In Comprehensive Organometallic Chemistry IV, (Elsevier), pp. 297–313. https://doi.org/10.1016/b978-0-12-820206-7.00032-9.

16. Bertrand, B., Stefan, L., Pirrotta, M., Monchaud, D., Bodio, E., Richard, P., Le Gendre, P., Warmerdam, E., de Jager, M.H., Groothuis, G.M.M., et al. (2014). Caffeine-based gold(I) N-heterocyclic carbenes as possible anticancer agents: Synthesis and biological properties. Inorg. Chem. *53*, 2296–2303. https://doi.org/10.1021/ic403011h.

17. Kaußler, C., Wragg, D., Schmidt, C., Moreno-Alcántar, G., Jandl, C., Stephan, J., Fischer, R.A., Leoni, S., Casini, A., and Bonsignore, R. (2022). "Dynamical docking" of cyclic dinuclear Au(I) bis-N-heterocyclic complexes facilitates their binding to G-quadruplexes. Inorg. Chem. *61*, 20405–20423. https://doi.org/10.1021/acs.inorgchem.2c03041.

18. Roder, C., and Thomson, M.J. (2015). Auranofin: Repurposing an old drug for a golden new age. Drugs R *15*, 13–20. https://doi.org/10.1007/s40268-015-0083-y.

19. Bindoli, A., Rigobello, M.P., Scutari, G., Gabbiani, C., Casini, A., and Messori, L. (2009). Thioredoxin reductase: A target for gold compounds acting as potential anticancer drugs. Coord. Chem. Rev. *253*, 1692–1707. https://doi.org/10.1016/j.ccr.2009.02.026.

20. Fan, C., Zheng, W., Fu, X., Li, X., Wong, Y.S., and Chen, T. (2014). Enhancement of auranofin-induced lung cancer cell apoptosis by selenocystine, a natural inhibitor of TrxR1 in vitro and in vivo. Cell Death Dis. *5*, e1191. https://doi.org/10.1038/cddis.2014.132.

21. Thomas, S.R., Bonsignore, R., Sánchez Escudero, J., Meier-Menches, S.M., Brown, C.M., Wolf, M.O., Barone, G., Luk, L.Y.P., and Casini, A. (2020). Exploring the chemoselectivity towards cysteine arylation by cyclometallated Au(III) compounds: New mechanistic insights. Chembiochem *21*, 3071–3076. https://doi.org/10.1002/cbic.202000262.

22. Bertrand, B., and Casini, A. (2014). A golden future in medicinal inorganic chemistry: The promise of anticancer gold organometallic compounds. Dalton Trans. *43*, 4209–4219. https://doi.org/10.1039/c3dt52524d.

23. Martínez-Calvo, M., and Mascareñas, J.L. (2018). Organometallic catalysis in biological media and living settings. Coord. Chem. Rev. *359*, 57–79. https://doi.org/10.1016/j.ccr.2018.01.011.

24. Tong, K.-C., Lok, C.-N., Wan, P.-K., Hu, D., Fung, Y.M.E., Chang, X.-Y., Huang, S., Jiang, H., and Che, C.-M. (2020). An anticancer gold(III)-activated porphyrin scaffold that covalently modifies protein cysteine thiols. Proc. Natl. Acad. Sci. *117*, 1321–1329. https://doi.org/10.1073/pnas.1915202117.

25. Tsubokura, K., Vong, K.K.H., Pradipta, A.R., Ogura, A., Urano, S., Tahara, T., Nozaki, S., Onoe, H., Nakao, Y., Sibgatullina, R., et al. (2017). In vivo gold complex catalysis within live mice. Angew. Chem. Int. Ed. *56*, 3579–3584. https://doi.org/10.1002/anie.201610273.

26. Thomas, S.R., and Casini, A. (2020). Gold compounds for catalysis and metal-mediated transformations in biological systems. Curr. Opin. Chem. Biol. *55*, 103–110. https://doi.org/10.1016/j.cbpa.2019.12.007.

27. Kung, K.K.Y., Ko, H.M., Cui, J.F., Chong, H.C., Leung, Y.C., and Wong, M.K. (2014). Cyclometalated gold(III) complexes for chemoselective cysteine modification via ligand controlled C-S bond-forming reductive elimination. Chem. Commun. *50*, 11899–11902. https://doi.org/10.1039/c4cc04467c.

28. de Paiva, R.E.F., Du, Z., Nakahata, D.H., Lima, F.A., Corbi, P.P., and Farrell, N.P. (2018). Gold-catalyzed C-S aryl-group transfer in zinc finger proteins. Angew. Chem. Int. Ed. *57*, 9305–9309. https://doi.org/10.1002/anie.201803082.

29. Wenzel, M.N., Bonsignore, R., Thomas, S.R., Bourissou, D., Barone, G., and Casini, A. (2019). Cyclometalated Au(III) complexes for cysteine arylation in zinc finger protein domains: Towards controlled reductive elimination. Chem. Eur J. *25*, 7628–7634. https://doi.org/10.1002/chem.201901535.

30. Casini, A., Guerri, A., Gabbiani, C., and Messori, L. (2008). Biophysical characterisation of adducts formed between anticancer metallodrugs and selected proteins: New insights from X-ray diffraction and mass spectrometry studies. J. Inorg. Biochem. *102*, 995–1006. https://doi.org/10.1016/j.jinorgbio.2007.12.022.

31. Geri, A., Massai, L., and Messori, L. (2023). Protein metalation by medicinal gold compounds: Identification of the main features of the metalation process through ESI MS experiments. Molecules *28*, 5196. https://doi.org/10.3390/molecules28135196.

32. Tong, K.-C., Hu, D., Wan, P.-K., Lok, C.-N., and Che, C.-M. (2020). Anticancer gold(III) compounds with porphyrin or N-heterocyclic carbene ligands. Front. Chem. *8*, 587207. https://doi.org/10.3389/fchem.2020.587207.

33. Schmidt, C., Zollo, M., Bonsignore, R., Casini, A., and Hacker, S.M. (2022). Competitive profiling of ligandable cysteines in Staphylococcus aureus with an organogold compound. Chem. Commun. *58*, 5526–5529. https://doi.org/10.1039/d2cc01259f.

34. Pushie, M.J., Pickering, I.J., Korbas, M., Hackett, M.J., and George, G.N. (2014). Elemental and chemically specific X-ray fluorescence imaging of biological systems. Chem. Rev. *114*, 8499–8541. https://doi.org/10.1021/cr4007297.

35. Davis, K.J., Carrall, J.A., Lai, B., Aldrich-Wright, J.R., Ralph, S.F., and Dillon, C.T. (2012). Does cytotoxicity of metallointercalators correlate with cellular uptake or DNA affinity? Dalton Trans. *41*, 9417–9426. https://doi.org/10.1039/c2dt30217a.

36. Lovett, J.H., and Harris, H.H. (2021). Application of X-ray absorption and X-ray fluorescence techniques to the study of metallodrug action. Curr. Opin. Chem. Biol. *61*,

135–142. https://doi.org/10.1016/j.cbpa.2020.12.004.

37. Casini, A., Vessières, A., and Meier-Menches, S.M. (2019). Metal-based Anticancer Agents ((Royal Society of Chemistry)). https://doi.org/10.1039/9781788016452.

38. Wenzel, M., and Casini, A. (2017). Mass spectrometry as a powerful tool to study therapeutic metallodrugs speciation mechanisms: Current frontiers and perspectives. Coord. Chem. Rev. *352*, 432–460. https://doi.org/10.1016/j.ccr.2017.02.012.

39. Meier, S.M., Gerner, C., Keppler, B.K., Cinellu, M.A., and Casini, A. (2016). Mass spectrometry uncovers molecular reactivities of coordination and organometallic gold(III) drug candidates in competitive experiments that correlate with their biological effects. Inorg. Chem. *55*, 4248–4259. https://doi.org/10.1021/acs.inorgchem.5b03000.

40. Hartinger, C.G., Groessl, M., Meier, S.M., Casini, A., and Dyson, P.J. (2013). Application of mass spectrometric techniques to delineate the modes-of-action of anticancer metallodrugs. Chem. Soc. Rev. *42*, 6186–6199. https://doi.org/10.1039/c3cs35532b.

41. Skos, L., Borutzki, Y., Gerner, C., and Meier-Menches, S.M. (2023). Methods to identify protein targets of metal-based drugs. Curr. Opin. Chem. Biol. *73*, 102257. https://doi.org/10.1016/j.cbpa.2022.102257.

42. Wang, H., Zhou, Y., Xu, X., Li, H., and Sun, H. (2020). Metalloproteomics in conjunction with other omics for uncovering the mechanism of action of metallodrugs: Mechanism-driven new therapy development. Curr. Opin. Chem. Biol. *55*, 171–179. https://doi.org/10.1016/j.cbpa.2020.02.006.

43. Zhou, Y., Li, H., and Sun, H. (2022). Metalloproteomics for biomedical research: methodology and applications. Annu. Rev. Biochem. *91*, 449–473. https://doi.org/10.1146/annurev-biochem-040320-104628.

44. Ha, J., Park, H., Park, J., and Park, S.B. (2021). Recent advances in identifying protein targets in drug discovery. Cell Chem. Biol. *28*, 394–423. https://doi.org/10.1016/j.chembiol.2020.12.001.

45. Meier, S.M., Kreutz, D., Winter, L., Klose, M.H.M., Cseh, K., Weiss, T., Bileck, A., Alte, B., Mader, J.C., Jana, S., et al. (2017). An organoruthenium anticancer agent shows unexpected target selectivity for plectin. Angew. Chem. Int. Ed. *56*, 8267–8271. https://doi.org/10.1002/anie.201702242.

46. Neuditschko, B., Legin, A.A., Baier, D., Schintlmeister, A., Reipert, S., Wagner, M., Keppler, B.K., Berger, W., Meier-Menches, S.M., and Gerner, C. (2021). Interaction with ribosomal proteins accompanies stress induction of the anticancer metallodrug BOLD-100/KP1339 in the endoplasmic reticulum. Angew. Chem. Int. Ed. *60*, 5063–5068. https://doi.org/10.1002/anie.202015962.

47. Neuditschko, B., King, A.P., Huang, Z., Janker, L., Bileck, A., Borutzki, Y., Marker, S.C., Gerner, C., Wilson, J.J., and Meier-Menches, S.M. (2022). An anticancer rhenium tricarbonyl targets Fe−S cluster biogenesis in ovarian cancer cells. Angew. Chem. Int. Ed. *61*, e202209136. https://doi.org/10.1002/anie.202209136.

48. Fung, S.K., Zou, T., Cao, B., Lee, P.-Y., Fung, Y.M.E., Hu, D., Lok, C.-N., and Che, C.-M. (2017). Cyclometalated gold(III) complexes containing N-heterocyclic carbene ligands engage multiple anti-cancer molecular targets. Angew. Chem. Int. Ed. *56*, 3892–3896. https://doi.org/10.1002/anie.201612583.

49. Wan, P.-K., Tong, K.-C., Lok, C.-N., Zhang, C., Chang, X.-Y., Sze, K.-H., Wong, A.S.T., and Che, C.-M. (2021). Platinum(II) N-heterocyclic carbene complexes arrest metastatic tumor growth. Proc. Natl. Acad. Sci. *118*, e2025806118. https://doi.org/10.1073/pnas.2025806118.

50. Sabatier, P., Beusch, C.M., Gencheva, R., Cheng, Q., Zubarev, R., and Arnér, E.S.J. (2021). Comprehensive chemical proteomics analyses reveal that the new TRi-1 and TRi-2 compounds are more specific thioredoxin reductase 1 inhibitors than auranofin. Redox Biol. *48*, 102184. https://doi.org/10.1016/j.redox.2021.102184.

51. Saei, A.A., Gullberg, H., Sabatier, P., Beusch, C.M., Johansson, K., Lundgren, B., Arvidsson, P.I., Arnér, E.S.J., and Zubarev, R.A. (2020). Comprehensive chemical proteomics for target deconvolution of the redox active drug auranofin. Redox Biol. *32*, 101491. https://doi.org/10.1016/j.redox.2020.101491.

52. Wang, H., Hu, L., Li, H., Lai, Y.-T., Wei, X., Xu, X., Cao, Z., Cao, H., Wan, Q., Chang, Y.-Y., et al. (2023). Mitochondrial ATP synthase as a direct molecular target of chromium(III) to ameliorate hyperglycaemia stress. Nat. Commun. *14*, 1738. https://doi.org/10.1038/s41467-023-37351-w.

53. Wang, H., Yan, A., Liu, Z., Yang, X., Xu, Z., Wang, Y., Wang, R., Koohi-Moghadam, M., Hu, L., Xia, W., et al. (2019). Deciphering molecular mechanism of silver by integrated omic approaches enables enhancing its antimicrobial efficacy in E. coli. PLoS Biol. *17*, e3000292. https://doi.org/10.1371/journal.pbio.3000292.

54. Wang, Y., Hu, L., Xu, F., Quan, Q., Lai, Y.-T., Xia, W., Yang, Y., Chang, Y.-Y., Yang, X., Chai, Z., et al. (2017). Integrative approach for the analysis of the proteome-wide response to bismuth drugs in Helicobacter pylori. Chem. Sci. *8*, 4626–4633. https://doi.org/10.1039/c7sc00766c.

55. Chiappetta, G., Gamberi, T., Faienza, F., Limaj, X., Rizza, S., Messori, L., Filomeni, G., Modesti, A., and Vinh, J. (2022). Redox proteome analysis of auranofin exposed ovarian cancer cells (A2780). Redox Biol. *52*, 102294. https://doi.org/10.1016/j.redox.2022.102294.

56. Dodson, M., de la Vega, M.R., Cholanians, A.B., Schmidlin, C.J., Chapman, E., and Zhang, D.D. (2019). Modulating NRF2 in disease: Timing Is everything. Annu. Rev. Pharm. Tox. *59*, 555–575. https://doi.org/10.1146/annurev-pharmtox-010818-021856.

57. Lu, Y., Ma, X., Chang, X., Liang, Z., Lv, L., Shan, M., Lu, Q., Wen, Z., Gust, R., and Liu, W. (2022). Recent development of gold(I) and gold(III) complexes as therapeutic agents for cancer diseases. Chem. Soc. Rev. *51*, 5518–5556. https://doi.org/10.1039/d1cs00933h.

58. Fritz-Wolf, K., Kehr, S., Stumpf, M., Rahlfs, S., and Becker, K. (2011). Crystal structure of the human thioredoxin reductase–thioredoxin complex. Nat. Commun. *2*, 383. https://doi.org/10.1038/ncomms1382.

59. Meier, S.M., Tsybin, Y.O., Dyson, P.J., Keppler, B.K., and Hartinger, C.G. (2012). Fragmentation methods on the balance: Unambiguous top–down mass spectrometric characterization of oxaliplatin–ubiquitin binding sites. Anal. Bioanal. Chem. *402*, 2655–2662. https://doi.org/10.1007/s00216-011-5523-0.

60. Angelucci, F., Sayed, A.A., Williams, D.L., Boumis, G., Brunori, M., Dimastrogiovanni, D., Miele, A.E., Pauly, F., and Bellelli, A. (2009). Inhibition of Schistosoma mansoni thioredoxin-glutathione reductase by auranofin: structural and kinetic aspects. J. Biol. Chem. *284*, 28977–28985. https://doi.org/10.1074/jbc.M109.020701.

61. Lechner, S., Müller-Ladner, U., Neumann, E., Spöttl, T., Schlottmann, K., Rüschoff, J., Schölmerich, J., and Kullmann, F. (2003). Thioredoxin reductase 1 expression in colon cancer: Discrepancy between in vitro and in vivo findings. Lab. Invest. *83*, 1321–1331. https://doi.org/10.1097/01.Lab.0000085189.47968.F8.

62. Jürgens, S., Scalcon, V., Estrada-Ortiz, N., Folda, A., Tonolo, F., Jandl, C., Browne, D.L., Rigobello, M.P., Kühn, F.E., and Casini, A. (2017). Exploring the C^N^C theme: Synthesis and biological properties of tridentate cyclometalated gold(III) complexes. Bioorg. Med. Chem. *25*, 5452–5460. https://doi.org/10.1016/j.bmc.2017.08.001.

63. Schmidt, C., Karge, B., Misgeld, R., Prokop, A., Franke, R., Brönstrup, M., and Ott, I. (2017). Gold(I) NHC Complexes: Antiproliferative Activity, Cellular Uptake, Inhibition of Mammalian and Bacterial Thioredoxin Reductases, and Gram-Positive Directed Antibacterial Effects. Chem. Eur J. *23*, 1869–1880. https://doi.org/10.1002/chem.201604512.

64. Wang, L., Yang, Z., Fu, J., Yin, H., Xiong, K., Tan, Q., Jin, H., Li, J., Wang, T., Tang, W., et al. (2012). Ethaselen: a potent mammalian thioredoxin reductase 1 inhibitor and novel organoselenium anticancer agent. Free Radic. Biol. Med. *52*, 898–908. https://doi.org/10.1016/j.freeradbiomed.2011.11.034.

65. Stafford, W.C., Peng, X., Olofsson, M.H., Zhang, X., Luci, D.K., Lu, L., Cheng, Q., Trésaugues, L., Dexheimer, T.S., Coussens, N.P., et al. (2018). Irreversible inhibition of cytosolic thioredoxin reductase 1 as a mechanistic basis for anticancer therapy. Sci. Transl. Med. *10*, eaaf7444. https://doi.org/10.1126/scitranslmed.aaf7444.

66. Jan, Y.-H., Heck, D.E., Gray, J.P., Zheng, H., Casillas, R.P., Laskin, D.L., and Laskin, J.D. (2010). Selective targeting of selenocysteine in thioredoxin reductase by the half mustard 2-chloroethyl ethyl sulfide in lung epithelial cells. Chem. Res. Toxicol. *23*, 1045–1053. https://doi.org/10.1021/tx100040k.

67. Zeisel, L., Felber, J.G., Scholzen, K.C., Poczka, L., Cheff, D., Maier, M.S., Cheng, Q., Shen, M., Hall, M.D., Arnér, E.S.J., et al. (2022). Selective cellular probes for mammalian thioredoxin reductase TrxR1: Rational design of RX1, a

modular 1,2-thiaselenane redox probe. Chem *8*, 1493–1517. https://doi.org/10.1016/j.chempr.2022.03.010.

68. Zhang, J., Zhang, B., Li, X., Han, X., Liu, R., and Fang, J. (2019). Small molecule inhibitors of mammalian thioredoxin reductase as potential anticancer agents: An update. Med. Res. Rev. *39*, 5–39. https://doi.org/10.1002/med.21507.

69. Zhang, B., Zhang, J., Peng, S., Liu, R., Li, X., Hou, Y., Han, X., and Fang, J. (2017). Thioredoxin reductase inhibitors: a patent review. Expert Opin. Ther. Pat. *27*, 547–556. https://doi.org/10.1080/13543776.2017.1272576.

70. Meier-Menches, S.M., Neuditschko, B., Zappe, K., Schaier, M., Gerner, M.C., Schmetterer, K.G., Del Favero, G., Bonsignore, R., Cichna-Markl, M., Koellensperger, G., et al. (2020). An organometallic gold(I) bis-N-heterocyclic carbene complex with multimodal activity in ovarian cancer cells. Chem. Eur J. *26*, 15528–15537. https://doi.org/10.1002/chem.202003495.

71. Schomburg, L., and Schweizer, U. (2009). Hierarchical regulation of selenoprotein expression and sex-specific effects of selenium. Biochim. Biophys. Acta *1790*, 1453–1462. https://doi.org/10.1016/j.bbagen.2009.03.015.

72. Touat-Hamici, Z., Bulteau, A.-L., Bianga, J., Jean-Jacques, H., Szpunar, J., Lobinski, R., and Chavatte, L. (2018). Selenium-regulated hierarchy of human selenoproteome in cancerous and immortalized cells lines. Biochim. Biophys. Acta *1862*, 2493–2505. https://doi.org/10.1016/j.bbagen.2018.04.012.

73. Lin, H.-C., Ho, S.-C., Chen, Y.-Y., Khoo, K.-H., Hsu, P.-H., and Yen, H.-C.S. (2015). SELENOPROTEINS. CRL2 aids elimination of truncated selenoproteins produced by failed UGA/Sec decoding. Science *349*, 91–95. https://doi.org/10.1126/science.aab0515.

74. Sporn, M.B., and Liby, K.T. (2012). NRF2 and cancer: The good, the bad and the importance of context. Nat. Rev. Cancer *12*, 564–571. https://doi.org/10.1038/nrc3278.

75. Ianevski, A., Giri, A.K., and Aittokallio, T. (2022). SynergyFinder 3.0: An interactive analysis and consensus interpretation of multi-drug synergies across multiple samples. Nucleic Acids Res. *50*, W739–W743. https://doi.org/10.1093/nar/gkac382.

76. Alaoui-Jamali, M.A., Bismar, T.A., Gupta, A., Szarek, W.A., Su, J., Song, W., Xu, Y., Xu, B., Liu, G., Vlahakis, J.Z., et al. (2009). A novel experimental heme oxygenase-1–targeted therapy for hormone-refractory prostate cancer. Cancer Res. *69*, 8017–8024. https://doi.org/10.1158/0008-5472.Can-09-0419.

77. Petrache, I., Otterbein, L.E., Alam, J., Wiegand, G.W., and Choi, A.M. (2000). Heme oxygenase-1 inhibits TNF-α-induced apoptosis in cultured fibroblasts. Am. J. Physiol. Lung Cell Mol. Physiol. *278*, L312–L319. https://doi.org/10.1152/ajplung.2000.278.2.L312.

78. Babak, M.V., Chong, K.R., Rapta, P., Zannikou, M., Tang, H.M., Reichert, L., Chang, M.R., Kushnarev, V., Heffeter, P., Meier-Menches, S.M., et al. (2021). Interfering with metabolic profile of triple-negative breast cancers using rationally designed metformin prodrugs. Angew. Chem. Int. Ed. *60*, 13405–13413. https://doi.org/10.1002/anie.202102266.

79. de Andrade Querino, A.L., de Sousa, A.M., Thomas, S.R., de Lima, G.M., Dittz, D., Casini, A., do Monte-Neto, R.L., and Silva, H. (2023). Organogold(III)-dithiocarbamate compounds and their coordination analogues as anti-tumor and anti-leishmanial metallodrugs. J. Inorg. Biochem. *247*, 112346. https://doi.org/10.1016/j.jinorgbio.2023.112346.

80. Kim, J.H., Ofori, S., Parkin, S., Vekaria, H., Sullivan, P.G., and Awuah, S.G. (2021). Anticancer gold(III)-bisphosphine complex alters the mitochondrial electron transport chain to induce in vivo tumor inhibition. Chem. Sci. *12*, 7467–7479. https://doi.org/10.1039/d1sc01418h.

81. Bertrand, B., Spreckelmeyer, S., Bodio, E., Cocco, F., Picquet, M., Richard, P., Le Gendre, P., Orvig, C., Cinellu, M.A., and Casini, A. (2015). Exploring the potential of gold(III) cyclometallated compounds as cytotoxic agents: variations on the C^N theme. Dalton Trans. *44*, 11911–11918. https://doi.org/10.1039/c5dt01023c.

82. Abás, E., Bellés, A., Rodríguez-Diéguez, A., Laguna, M., and Grasa, L. (2021). Selective cytotoxicity of cyclometalated gold(III) complexes on Caco-2 cells is mediated by G2/M cell cycle arrest. Metallomics *13*, mfab034. https://doi.org/10.1093/mtomcs/mfab034.